Applied Geochemistry 126 (2021) 104881

Contents lists available at ScienceDirect

Applied Geochemistry

journal homepage: http://www.elsevier.com/locate/apgeochem

Signs of in-situ geochemical interactions at the granite–concrete interface of a radioactive waste disposal

Zsuzsanna Szabó-Krausz [a,b,*], László Előd Aradi [a], Csilla Király [c], Péter Kónya [d], Patrik Török [e], Csaba Szabó [a], György Falus [d]

[a] Lithosphere Fluid Research Lab, Department of Petrology and Geochemistry, Eötvös Loránd University, Pázmány P. S. 1/C, 1117, Budapest, Hungary
[b] MTA Premium Postdoctorate Research Program, Hungarian Academy of Sciences and Eötvös Loránd Research Network, Budapest, Hungary
[c] Geographical Institute, Research Centre for Astronomy and Earth Sciences, Budaörsi út 45., 1112, Budapest, Hungary
[d] Mining and Geological Survey of Hungary, Stefánia út 14., 1143, Budapest, Hungary
[e] Public Limited Company for Radioactive Waste Management, P.O. Box 12., 7031, Paks, Hungary

ARTICLE INFO

Handling editor: Dr. Z Zimeng Wang

Keywords:
Radioactive waste disposal
Geochemical interactions
Granite–concrete interface
Raman-map

ABSTRACT

Eleven unique core samples from the National Radioactive Waste Repository of Hungary, Bátaapáti were studied in this work. The samples all cross the granite–concrete interface and have been drilled from around 275 m depth from the surface, 1–15 months after concrete injection. Phase analytical techniques, optical microscopy, SEM-EDS and Raman-spectroscopy were used for the analysis of interactions between granitic rock and cementitious building material. Newly formed phases, Ca-carbonates and titanite, were observed at the interface. Carbonation may reduce the porosity and permeability in the contact zone. The presence of titanite indicates the changing geochemical and thermodynamical constrains along the reaction front of granite–concrete, furthermore, it may help in the validation of future geochemical models. The cementitious material is seen to penetrate among the sheets of biotite mineral in granite which process is probable to cause the attachment of granite and concrete.

1. Introduction

Cement and concrete are structural materials used in radioactive waste repositories. In some designs, these materials are also responsible for preventing fluid migration out of the complex and, therefore, minimize the mobilization of radionuclides (Koťátková et al., 2017). This requires concrete to keep its physical and chemical integrity for as long as possible in the ambient geological conditions. The time for which radioactive waste disposals should be designed is a matter of debate, but it ranges from 1000 to 100 000 years (Moghissi, 2006; Murray et al., 2020; Siren et al., 2015). For all of these orders of magnitude, it is difficult to provide predictions on the state of building materials and the interacted host rock itself.

Three research pathways are available for the assessment of geochemical reactions in such systems; these are laboratory experiments, in-situ studies and numerical geochemical modeling, preferably validated by results of foregoing experimental works. As a type of in-situ studies, the investigation of interfaces between rock or bentonite and concrete, prepared in special conditions in underground laboratories, can be mentioned. Such studies have been performed at the Grimsel Test Site (Alonso et al., 2017; Fernández et al., 2017), in the Mont-Terri Rock Laboratory (Bernard et al., 2020; Dauzeres et al., 2016; Jenni et al, 2014, 2017; Lerouge et al., 2017) and at the Tournemire experimental station (Lalan et al, 2016, 2019). The advantages are the long experimental times (1–13 years) and that the conditions are much closer to the reality than in laboratory batch experiments (even after adjusted pressure and temperature reactor experiments, artefacts may form while ambient conditions are reached again in a short time). Interface samples relevant for radioactive waste disposals are also prepared and investigated in some other laboratory experiments (Balmer et al., 2017; Fernández et al., 2006). Geochemical modeling has also focused on interfaces is many cases (Dauzeres et al., 2016; De Windt et al., 2008; Fernández et al., 2006; Idiart et al., 2020; Jenni et al., 2017) showing the importance of such samples in understanding geochemical interactions between two substances, the bedrock and building material.

Granite host rock is investigated for the deep geological disposal of low- and medium-level or high-level radioactive waste in many countries. Several papers can be found from e.g. China (Wang et al., 2018;

* Corresponding author. Department of Petrology and Geochemistry, Eötvös Loránd University, Pázmány P. s. 1/C, 1117 Budapest, Hungary
E-mail addresses: szabo.zsuzsanna@ttk.elte.hu, zsszabo86@gmail.com, zabo86@gmail.com (Z. Szabó-Krausz).

https://doi.org/10.1016/j.apgeochem.2021.104881
Received 16 September 2020; Received in revised form 4 December 2020; Accepted 6 January 2021
Available online 12 January 2021

Zuo et al., 2017), Finland (Siren et al., 2015; Soler, 2012; Soler et al., 2011), France (Parneix, 1992), India (Gautam et al., 2019), Japan (Yoshida et al., 2000), South Korea (Jo et al., 2019), Spain (Alonso et al., 2017; Buil et al., 2010; Fernández et al., 2017; Lu et al., 2012; Samper et al., 2016), Sweden (Hedin and Olsson, 2016) and the USA (Mariner et al., 2011) dealing with different aspects of theoretical, planned or existing repositories in granite. In many of the designs, especially in high-level waste repositories, bentonite has the main role as building material in the engineered barrier system. This increased the interest in the research of geochemical interactions between granite and clay (Buil et al., 2010; Samper et al., 2016). Other designs apply concrete as the barrier against fluid flow (Koťátková et al., 2017). Therefore, the need of understanding geochemical processes in the granite and alkaline plume (derived from the cement pore water), cement or concrete system also appears in international research publications (Chaparro et al., 2017; Pfingsten et al., 2006; Soler and Mäder, 2007, 2010). However, no published study of granite–concrete interface samples has been found by the authors. The closest subjects seem to be the bentonite–concrete interface affected by granitic pore water prepared at the Grimsel Test Site (Alonso et al., 2017; Fernández et al., 2017).

Granite is also the host rock in the National Radioactive Waste Repository of Hungary, Bátaapáti. The geochemical interactions between granite and concrete in this already opened disposal site have been previously examined both in experimental and independent 1D thermodynamical reactive transport modeling studies. However, the record of these only appear in a report, a local conference proceeding and a M. Sc. thesis written in Hungarian (Benő and Molnár, 2010; Fintor and Nagy, 2015; Nagy, 2015) and they have not been published for the international research community. Also, as emphasized previously, the study of interface can bring important insights into understanding the geochemical process in the granite–concrete system, but such samples from the site were not examined before, just like none was reported about from any other existing or planned repositories in the world, in the best knowledge of the authors.

The main aims of present work are to find, summarize and evaluate the signs of geochemical interactions in core samples of the granite–concrete interface from the National Radioactive Waste Repository of Hungary, Bátaapáti, which is a functioning repository of medium and low level waste. This paper is not only the first peer-reviewed international publication about geochemical interactions in the repository at Bátaapáti, but it is also the first one focusing on samples of interfaces of granite and concrete. The findings of this research will also provide important considerations for the improvement of predictive modeling work in the studied and similar repositories.

2. Study site and cores

The National Radioactive Waste Repository of Hungary has been hosting medium and low level waste since 2012. It is located in Bátaapáti, S-Hungary (Fig. 1A) at a depth of 200–300 m, where the temperature varies around 17–18 °C. The complete chamber field of the repository can be seen in Fig. 1B. The chamber walls are made in the rock body of the Mórágy Granite Formation (Fig. 1C) by the use of 40 cm thick shotcrete with steel reinforcing mesh and the chambers, when closed, are also filled with concrete.

The purpose of the studied shotcrete in the repository was mechanical support. Information about the preparation and original ingredients of this material are summarized below following the construction plan document (Nehme, 2013). The recommended composition of the shotcrete was as follows: 72.5 wt% aggregate (65 wt% of which is sand and 35 wt% is gravel including granitic rock fragments), 18.8 wt% CEM I 42, 5 N Portland Cement, 7.5 wt% water giving a water to cement ratio of 0.4, additives such as 0.2 wt% Viscocrete SC 305 AT and at the site, 0.9 wt% Sigunit –L-AF. The latter is a mixture of special organic substances based on its product data sheet (Sika, 2019).

The granitoid massif was described by Király and Koroknai (Király,

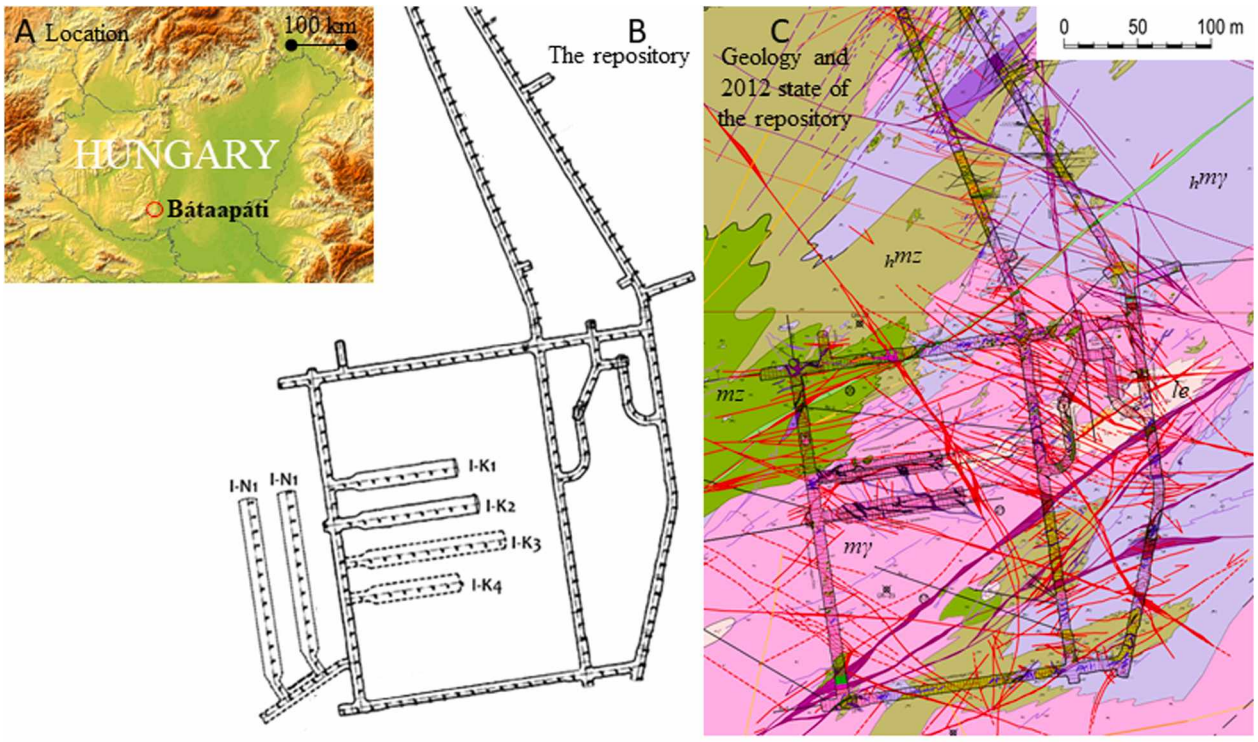

Fig. 1. *A) The location of the National Radioactive Waste Repository at Bátaapáti, Hungary on the geographical map of the Pannonian Basin. B) Complete chamber field of the repository (modified after Kereki, 2016) C) Geology of the area with the 2012 state of the repository (Maros et al., 2012). The purple and red lines represent first and second order fractures, respectively. Rock types: mγ – monzogranite, hmγ – hybrid monzogranite, le – leucocratic monzogranite, mz – monzonite, hmz – hybrid monzonite.* (For interpretation of the references to color in this figure legend, the reader is referred to the Web version of this article.)

2010; Király and Koroknai, 2004) in means of mineralogical, petrographic and geochemical properties and it consists of dominantly monzogranite intercalated with a more mafic variety of monzonitic composition (Fig. 1C, Maros et al., 2012). The fracture network characteristics vary remarkably with lithology (M. Tóth, 2018). The body is divided into poorly deformed and intensively fractured zones. Due to late mineralization, some of these fractures are clogged, and multigenerational calcite veins are described (Balla et al., 2009), whereas others function as migration pathways (M. Tóth, 2018) of the pore fluid. There is a significant first order fracture in the repository, which goes along a SW-NE direction (Fig. 1C) and this provides a barrier against fluid flow as a clogged fracture. Based on solution composition measurements (Benő and Molnár, 2010; Szabó et al., 2017), the formation water typically contains about 30–40 mg/l Na^+, Ca^{2+} and Mg^{2+} as the most important cations, and around 350 mg/l HCO_3^- as the main anion. The dissolved silica content is about 30 mg/l (given as H_2SiO_3).

Core samples from the repository were taken between 2014 and 2015 for monitoring the transmissivity in the Excavation Damage Zone (EDZ). Eleven of these cores, which cross the granite–concrete interface (Table 1), became available for this geochemical perspective study. All of these cores originate from the I–K3 and I–K4 chambers of the repository (Fig. 1B, Table 1). The drilling happened at variable, 3–67 m distances from the entrance of the chambers and at a maximum 12.3 m above sea level (around at 275 m depths from the surface, Table 1). Ages of interfaces vary from 20 to 455 days (Table 1) representing the elapsed time between concrete injection and coring and, therefore, the duration of geochemical reactions in the subsurface. The cores can be divided into two main types depending on the attachment of granite and concrete, i.e. if they are grown together or separated from each other (Fig. 2, Table 1). The samples were stored at room temperature and at atmospheric pressure in dry conditions and got available for the aims of this study in 2017 and the preparation of samples, detailed below, started then.

3. Methods

3.1. Sample preparation

Two sets of samples were prepared from the eleven cores. These sets are 1, powder samples for phase analytics and 2, ordinary thin sections for study by imaging techniques. The number of samples prepared by cores and their type are summarized in Table 2. The <63 μm grain size powder samples (1) were taken from the granite, concrete parts of all eleven cores and also from the interfaces, separately. The granite and concrete were sampled by selecting and crushing a representative part of the materials. Whereas, the interface was sampled either by a dental drill or by scratching. Scratching was typically applied for non-attached cores (Fig. 2B). The thin sections (2) were prepared of the interfaces directly when possible (attached cores, Figs. 2A and 3A). For non-attached cores (Fig. 2B), two thin sections were made of the edges of granite and concrete, separately (Fig. 3B). All of the prepared samples (sets 1, 2) were stored in three layers of plastic bags in ambient conditions until their analysis.

Table 1
The studied granite–concrete cores available from the National Radioactive Waste Repository and information about their origin: the chambers (Fig. 1B), the drilling distances from the entrance of the chambers, the elevations above sea level, the ages representing the elapsed time between concrete injection and coring and the type of cores (grown together or not, Fig. 2).

Core ID	Chamber	Distance (m)	Elevation (mBf)	Age (days)	Grown together
Bz-1521	I–K3	8.3	7.2	455	Yes
Bz-1531	I–K3	8.9	4.1	454	Yes
Bz-1533	I–K3	8.8	2.9	453	No
Bz-1542	I–K3	3.2	4.1	451	No
Bz-1621	I–K4	8.3	7.3	308	No
Bz-1642	I–K4	13.1	3.8	305	No
Bz-1721	I–K3	26.3	10.5	20	Yes
Bz-1753	I–K3	29.9	1.8	282	Yes
Bz-1812	I–K4	65.3	10.9	57	Yes
Bz-1843	I–K4	64.2	12.3	58	Yes
Bz-1862	I–K4	66.6	3.1	56	Yes

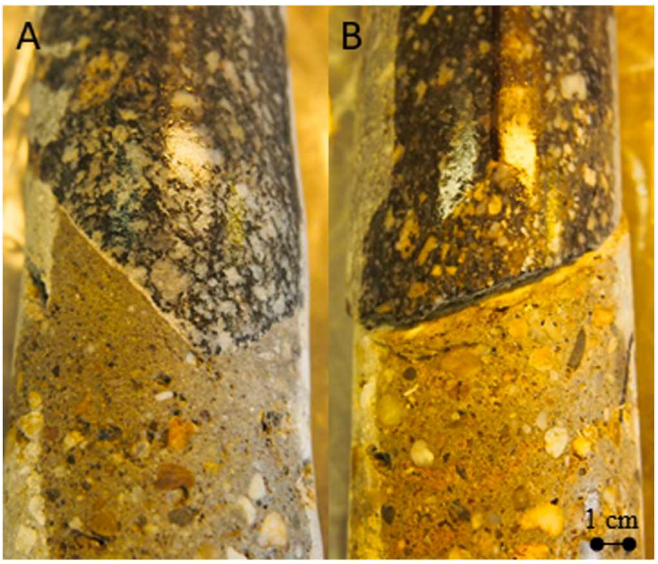

Fig. 2. Representative examples for the main types of core samples; cores in which granite and concrete A) are grown together along the interface, B) are not grown together but their interface can be reconstructed.

3.2. Phase and geochemical analytical methods

For chemical composition analysis, after dissolution of the powdered materials, Inductively Coupled Plasma-Optical Emission Spectrometry (ICP-OES), a HORIBA Jobin Yvon® ULTIMA 2C instrument was used. The determination of carbonate content happened by a calcimeter, which works in accordance with the method of Scheibler and measures the pressure of CO_2 gas produced from reaction with HCl. The hygroscopic water content was gained by the recording the weight difference before and after heating the samples up to 105 °C and the structural water content after up to 1050 °C. For phase, i.e. mineral composition analysis techniques of X-Ray Diffraction (XRD) by a Philips® PW 1730 instrument; Attenuated Total Reflectance Fourier Transform Infrared Spectroscopy (ATR-FTIR) by a Bruker® Vertex 70 instrument with Bruker® Platinum single reflection diamond ATR module and mercury-cadmium-telluride detector; and Thermal Analysis (TA) by a MOM® Derivatograph-C instrument were applied. Only XRD measurement was performed on all samples, the ATR-FTIR and TA analyses were done on

Table 2
Number of studied powder samples and thin sections by core.

Core ID	Number of prepared samples	
	Powder	Thin section
Bz-1521	3*	1*
Bz-1531	3*	1*
Bz-1533	4*	4
Bz-1542	3*	2
Bz-1621	4*	2
Bz-1642	3*	2
Bz-1721	4*	1*
Bz-1753	2	2*
Bz-1812	3*	1*
Bz-1843	3*	2*
Bz-1862	3*	2
Total	*35*	*20*

*includes one sample of the interface itself

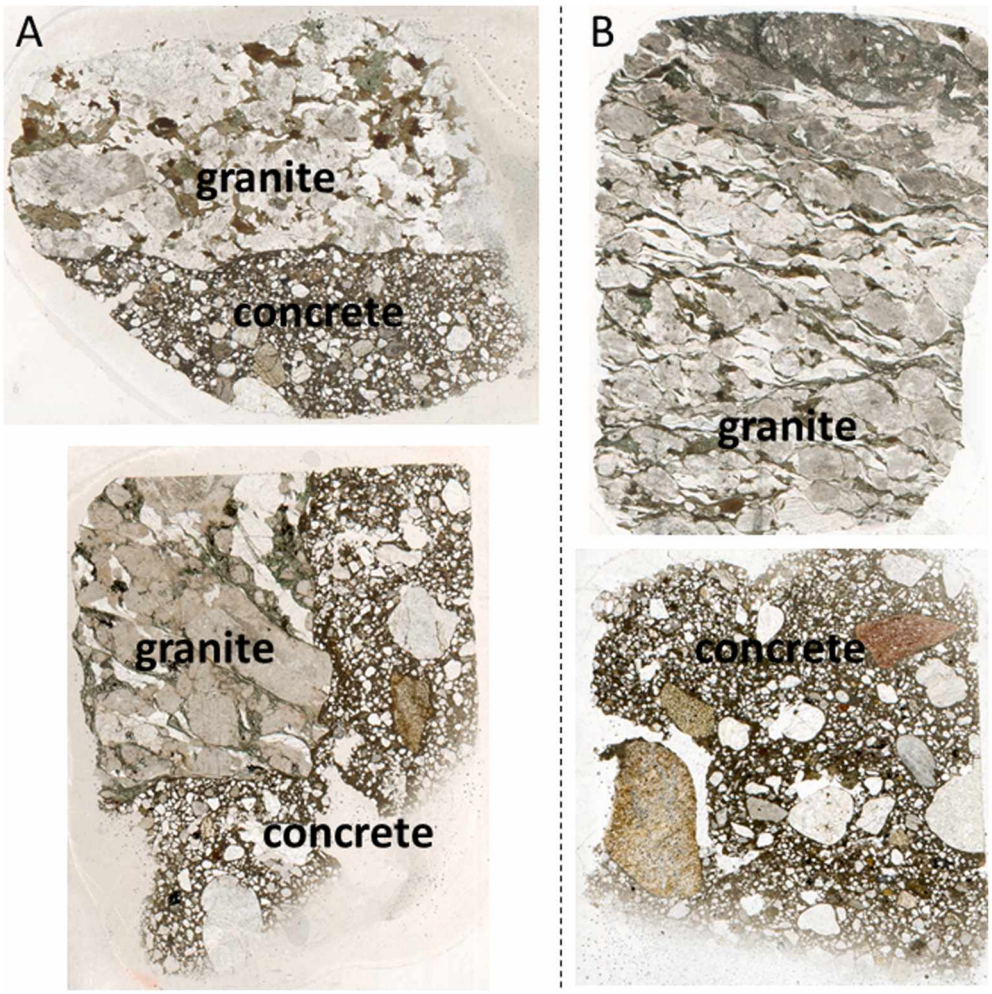

Fig. 3. Representative examples of thin sections made of the main types of core samples; cores in which granite and concrete A) are grown together along the interface – two samples in two thin sections, B) are not grown together but their interface can be reconstructed – granite and concrete parts of one sample in two thin sections.

selected powdered samples. All of these analyses were carried out in the laboratories of the Mining and Geological Survey of Hungary, Budapest.

3.3. Imaging techniques and point analysis

On thin sections, optical microscopy by a Nikon® Eclipse LV100 POL polarizing microscope and scanning electron microcopy together with energy-dispersive X-ray spectroscopy (SEM-EDS) was applied. The latter investigation was done using two instruments: an Amray® 1830 I/T6 coupled with EDAX PV 9800 and a Hitachi® TM4000Plus instrument. Raman-microspectroscopy measurements were carried out with a Horiba LabRAM HR800 equipped with an Olympus BXFM microscope. During both the point measurements and Raman mapping the Nd-YAG laser (532 nm) was focused with a 50 × objective on the sample surface, using 600 grooves/mm optical grating. These techniques were available for the aims of this study in the Lithosphere Fluid Research Lab and through the Research and Industrial Relations Center of Eötvös Loránd University, Budapest.

4. Results

4.1. Results of phase analytics

The chemical composition of the concrete part of the cores was determined for supporting the identification of its mineral composition. Four samples were selected for such analysis assuming their representativity. The results of this concrete chemical analysis by ICP-OES are summarized in Table 3.

The concrete consists of dominantly SiO_2 (55–65 wt%) mainly due to its high quartz sand content. The second most abundant chemical component is CaO (17–23 wt%) mainly consisted in the clinker phases in cement. Furthermore, Al_2O_3 (3–4 wt%), Fe_2O_3 (1–2 wt%), SO_3 (~1 wt %), MgO (~1 wt%), K_2O (0.5–1 wt%), Na_2O (~0.5 wt%), TiO_2 (0.1–0.2 wt%) and MnO (~0.1 wt%) are determined with decreasing contributions. Even less BaO and SrO (0.01–0.02 wt%) are detected (Table 3). Approximately 3 wt% of CO_2 is released in the analysis originating from carbonate minerals and ~5 wt% structural water is detected (Table 3), which is derived from hydrate minerals (calcium [-aluminium] silicate hydrates, C(A)SH) of hardened cement.

The results of XRD, ATR-FTIR and TA analyses are summarized in Tables 4–6, respectively. Mineral composition of the granite is quite heterogeneous (Tables 4 and 5), probably due to sampling heterogeneity. However, the main phases generally are quartz, K-feldspar, plagioclase, mica and chlorite. In some samples, muscovite, amphibole and calcite were also detected.

The main phases in the cementitious part of the cores are also quartz, K-feldspar and plagioclase (Tables 4–6), which must relate to the sand and granitic rock fragments added to the shotcrete composition. Cement phases detected are ettringite, portlandite and remaining clinker, larnite. Neither of the methods was capable to detect the amorphous or

Table 3
Bulk chemical compositions, i.e. wt% proportions of elements and water contents in selected powder samples of concrete (C).

Powder sample/wt% of elements	SiO_2	TiO_2	Al_2O_3	Fe_2O_3	MnO	CaO	MgO	Na_2O	K_2O	SO_3	BaO	SrO	CO_2	hyg. H_2O	str. H_2O
Bz-1521-C	62.8	0.174	3.86	1.55	0.078	18.4	0.767	0.542	0.716	0.903	0.022	0.013	2.75	2.45	4.87
Bz-1621-C	61.8	0.177	3.94	1.40	0.079	18.7	0.754	0.564	0.660	1.040	0.023	0.012	2.85	2.73	5.18
	64.4	0.159	3.79	1.36	0.071	17.2	0.728	0.540	0.585	0.968	0.020	0.011	3.11	2.42	4.57
Bz-1753-C	55.2	0.193	3.95	1.48	0.106	22.5	1.120	0.513	0.844	1.140	0.025	0.013	3.59	3.37	5.90

microcrystalline C(A)SH gel, which usually consists of about the 50 wt% of the hydrated concrete matrix (e.g. Szabó-Krausz et al., 2020). Carbonates are also detected up to 9 wt% calcite, 3 wt% dolomite and 5 wt% vaterite.

The phases detected in the drilled or scratched interface samples (Tables 4–6) are a mixture of granite and concrete phases due to the non-exclusive sampling procedure. However, when significantly higher or lower modal proportions are determined than in the pure rock or building material, it is indicative of the composition of the minerals formed along the interface and of interaction of concrete and granite. Based on the semi-quantitative XRD and TA results (Tables 4 and 6), the main phases shown to precipitate at the interface are calcite and vaterite. These minerals are detected in increased amounts, up to 36 wt % and 16 wt%, respectively, in almost all of the measured interface powder samples. Besides calcite and vaterite, dolomite and aragonite are other carbonates occurring in some of the samples. However, not only carbonates are present in these materials, but in one sample also gypsum was confirmed by all three phase analytical techniques (Tables 4–6) and in other samples ackermanite, smectite, kaolinite, stratlingite or amorphous phases were detected by XRD (Table 4).

4.2. Results of imaging

4.2.1. Carbonate veins along or near the interface

As described by earlier works (Balla et al., 2009; Király, 2010; Király and Koroknai, 2004; M. Tóth, 2018; Maros et al., 2012) and summarized in Section 2, the granitoid massif of the area has an extended fracture network, in which hydrothermal calcite veins frequently appear (Balla et al., 2009). These veins in granite were observed by optical microscopy and SEM-EDS in some of the samples of this study (Fig. 4) and their identification was supported by Raman-microspectroscopy. Petrographic observations of these calcite veins, and the fact that they so frequently appear along the granite–concrete contact confirm that they cannot be always the results of random cracking when the repository chambers were made. Calcite veins along or near the interface are presented in Fig. 5A, C, D and E. A high variation was identified in the thickness of these veins ranging up to around 400 μm (Fig. 5E.), if they appear.

4.2.2. Titanium mineral precipitation in the contact zone

Two Ti-bearing phases were identified in thin sections of core samples by SEM-EDS and Raman-microspectroscopy. One of them is anatase (TiO_2) in the granite, shown in Figs. 1, 2 and 4 cm away from the contact zone. The Raman-spectrum of anatase is shown in Fig. 6. Anatase grains were also observed near the granite–concrete contact within biotite flakes, shown as the brightest grains in Fig. 7A.

The other Ti-phase is the titanite ($CaTiSiO_5$). This mineral was quite frequently detected along or near the granite–concrete interface, in the granite side (Fig. 5A, B, D and F). Raman-microspectroscopy also supported the identification of titanite occurrences (Fig. 6).

4.2.3. Cement within the layers of biotite in the granite

Biotite is a common phyllosilicate mineral in granite. Mica is detected by XRD in average 11 ± 7 wt% in the powered granite samples of this study (Section 4.1., Table 4) and in granite samples, it is identical to biotite. Therefore, it frequently appears just at the granite–concrete contact in the thin sections of interfaces. It was observed during the SEM-EDS investigations that the concrete matrix (hardened cement paste) penetrates biotite sheets/flakes along cleavage plains. Two typical examples can be seen in Fig. 7A and B where the combined element maps show the presence of cementitious materials even in up to about 50 μm depth in the biotite.

4.2.4. Two types of concrete matrix

Based on optical and electron microscopic observations of thin sections, the concrete near the interface can be generally divided into two zones depending on the distance from granite. In BSE images (Fig. 8) these two types of concrete matrices are seen as a lighter grey zone near the granite contact or the calcite vein at the interface (Fig. 8A) and a darker grey part further away. It was shown by EDS analysis at several locations in the thin sections, that with the distance from the contact with the granite, the Ca- and the K-content of the concrete matrix is decreasing, whereas its Si-, S- and Mg-content increases (Fig. 8A and B).

The reason for the most characteristic Ca-content variations might be found by looking at the Raman-map (Fig. 8B), which presents a similar location to BSE 1200x image. Based on the phase distribution, the elevated Ca-content in the concrete matrix is present in the newly formed, fine grained mineral, vaterite ($CaCO_3$), which precipitated in the pores of concrete. Therefore, it decreases the relative abundance of other elements. Note that Raman-spectroscopy detected organic matter (Fig. 8B), which is most probably the Sigunit –L-AF additive in concrete.

5. Discussion

5.1. Review of relevant literature

5.1.1. Observations in other experimental interface studies

Experimental interfaces studies in relevance of radioactive waste disposal have been done in connection with the interaction of clayey and cementitious materials. The clayey material is either bentonite (Alonso et al., 2017; Balmer et al., 2017; Fernández et al, 2006, 2017) or a clayey host rock (Bernard et al., 2020; Dauzeres et al., 2016; Jenni et al, 2014, 2017; Lalan et al, 2016, 2019; Lerouge et al., 2017). The bentonite in such experiments represents a part of the engineered barrier system. These bentonite–cement/concrete samples have been prepared either in surface laboratories (Balmer et al., 2017; Fernández et al., 2006) or at the Grimsel Test Site (Alonso et al., 2017; Fernández et al., 2017) in granitic environment. In the other studies, the clayey host rock can be characterized as argillaceous claystone or argillite. These kind of clayey host rock–cement/concrete experiments were carried out in the Mont-Terri Rock Laboratory (Bernard et al., 2020; Dauzeres et al., 2016; Jenni et al, 2014, 2017; Lerouge et al., 2017) and at the Tournemire experimental station (Lalan et al, 2016, 2019). The cementitious materials used are either concretes (Dauzeres et al., 2016; Jenni et al, 2014, 2017; Lerouge et al., 2017), shotcretes (Alonso et al., 2017; Dauzeres et al., 2016; Fernández et al., 2017; Jenni et al., 2014), mortars (Fernández et al., 2006) or cement pastes (Balmer et al., 2017; Bernard et al., 2020; Lalan et al, 2016, 2019), determined by the type of cement and the addition of superplasticizers, gravel and sand.

Reviewing the results of above studies, a few important findings seem to appear regularly. One of them is that in some of the samples a Mg-rich phase precipitates at the interface. This is either described as a

Table 4
Semi-quantitative XRD results, i.e. wt% proportions of phases detected in powder samples of granite (G), concrete (C), granite–concrete (GC) and concrete–concrete (CC) interface.

Powder sample /wt% of minerals		Silicates						
		quartz SiO_2	K-feldspar $KAlSi_3O_8$	plagioclase $Na_{0.5}Ca_{0.5}Si_3AlO_8$	mica $K(Mg_3,Al_2)AlSi_3O_{10}(OH)_2$	chlorite $Mg_5Al_2Si_3O_{10}(OH)_8$	amphibole $Ca_2Mg_4Al_{0.75}Fe_{0.25}(Si_7AlO_{22})(OH)_2$	ackermanite $Ca_2MgSi_2O_7$
Granite	Bz-1521-G	23	17	37	7	9		
	Bz-1531-G	15	20	43	15		3	
	Bz-1533-G	15	24	45	9	5		
	Bz-1542-G	9	47	34	5	4	1	
	Bz-1621-G	9	33	38	5	15		
	Bz-1642-G	6	46	37	5	3	2	
	Bz-1721-G	11	17	36	3	32		
	Bz-1753-G	19	27	32	15	7		
	Bz-1812-G	4	19	47	26		4	
	Bz-1843-G	19	26	36	17		2	
	Bz-1862-G	18	26	36	17	1	2	
Concrete	Bz-1521-C	55	7	7				
	Bz-1531-C	59	8	8	10			
	Bz-1533-C	69	7	10				
	Bz-1542-C	75	3	4	6		2	
	Bz-1621-C	56	5	9				
		59	4	8				
	Bz-1642-C	55	5	9	9	4	4	
	Bz-1721-C	53	6	8		4		
		50	5	13				
	Bz-1753-C	46	5	11				
	Bz-1812-C	74	6	6				
	Bz-1843-C	51	5	11				
	Bz-1862-C	57	6	8	7	4		
Interface	Bz-1521-GC	35	5	13	7			
	Bz-1531-GC	36	6	9	20			
	Bz-1533-GC	13	8	19	10		2	
	Bz-1533-CC	38	2	6				
	Bz-1542-GC	27	2	5	7		3	
	Bz-1621-GC	41	4	13				6
	Bz-1642-GC	38	5	6	5	6	t	
	Bz-1721-GC	37	16	13		9		
	Bz-1812-GC	26						
	Bz-1843-GC	30	6	10	28	2		
	Bz-1862-GC	28	9	19	7			

"tri-octahedral Mg sheet silicate" resulting from the transformation of montmorillonite in bentonite (Fernández et al., 2017) or a "tri-octahedral 2:1 phyllosilicate" resulting from the trioctahedralisation of smectite dioctahedral sheets (Lerouge et al., 2017). A more different "Mg–Si gel-like phase", identified as magnesium silicate hydrate (MSH) was also identified (Dauzeres et al., 2016). A new, probably MSH phase is also mentioned in the most recent study to date (Bernard et al., 2020). Magnesium zonation also appears in some of the other studies (Alonso et al., 2017; Jenni et al, 2014, 2017). Results refer to a process, in which Mg from the clayey material migrates into the cementitious phase (Alonso et al., 2017; Jenni et al., 2014). This is also supported by observations of Mg enrichment in the clay detached from the interface (Jenni et al., 2017). Besides MSH (Bernard et al., 2020; Dauzeres et al., 2016), other studies identify C(A)SH or its more crystalline form, tobermorite precipitated in the contact zone (Fernández et al., 2006; Lalan et al, 2016, 2019; Lerouge et al., 2017). However, calcium silicate hydrate (CSH) alteration and resulting loss of compactness also occurs (Alonso et al., 2017; Bernard et al., 2020).

Several articles (Bernard et al., 2020; Fernández et al., 2017; Jenni et al, 2014, 2017; Lalan et al, 2016, 2019) report of heterogeneous, zoned or diffuse carbonation (carbonate, mostly calcite precipitation) at the interface. This process needs dissolved Ca^{2+}, which is supplied from the dissolution of portlandite, and also of C(A)SH or ettringite. These dissolution processes are called as the decalcification of cement (Jenni et al., 2017; Lalan et al, 2016, 2019). The carbonate precipitation also requires the presence of dissolved CO_2, i.e. HCO_3^- and CO_3^{2-} ions in the solution. Either an atmospheric effect can be considered or the original composition of local pore waters. According to studies of Bernard et al. (2020), Jenni et al. (2017, 2014) and Lalan et al. (2019, 2016), the carbonation is linked to a decrease in porosity, i.e. pore clogging, which may avoid further alteration of the materials at greater depths.

Another general observation in reviewed articles connects to reactions of sulfate, SO_4^{2-}. In two of the articles SO_4^{2-} is described to diffuse from bentonite to concrete (Alonso et al., 2017; Fernández et al., 2017). This was linked to the presence of ettringite. Sulfate precipitation simply at the interface has also been observed (Lerouge et al., 2017). In contrary, it was also explained by Jenni et al. (2014) that in their experiments SO_4^{2-} rather diffused away because of the pH decrease at the interface causing the instability of ettringite. The released SO_4^{2-} then claimed to diffuse to higher pH environments in concrete. They later changed this hypothesis based on modeling results (Jenni et al., 2017) and said that portlandite and ettringite formation near the interface is restricted probably because of a shortage in Ca^{2+}. Bernard et al. (2020) also described the dissolution of ettringite in cement at the contact with the clayey rock.

5.1.2. *An overview of findings in granite–concrete studies*

As noted in the introduction, no published study of especially

Silicates		Cement phases					Carbonates				amorphous
smectite $(Na, Ca)_{0.33}(Al, Mg)_2(Si_4O_{10})$	kaolinite $Al_2Si_2O_5(OH)_4$	larnite Ca_2SiO_4	portlandite $Ca(OH)_2$	ettringite $Ca_6Al_2(SO_4)_3(OH)_{12}{:}26H_2O$	gypsum $CaSO_4{:}2H_2O$	stratlingite $Ca_2Al_2(SiO_2)(OH)_{10}{:}2.5H_2O$	calcite $CaCO_3$	vaterite $CaCO_3$	aragonite $CaCO_3$	dolomite $CaMg(CO_3)_2$	
							7				
							4				
							2				
							1				
							1				
		12	4	8			5			2	
			3				7	2		3	
			4				5	2		3	
			4				4	2			
		8	4	10			6	2			
		9	4	10			4	2			
			4				6	2		2	
		7	4	8			8	2			
		15	5	4			8				
		10	6	10			5			3	4
							9	5			
		17	4	4			5			3	
3			4				5	3		3	
		4	2	5			21				8
		5	4				16	4			
		9	6				33				
				6		7	29	6		6	
8		5	2				25	14		2	
				8	6		13	4	5		
	t	2					22	14		2	
			3	4			5	2		2	9
26											
	1	5	2				17	2		1	
			2	1			32				

granite–concrete interfaces has been found in the literature. Only one of the above reviewed articles of interface samples (Alonso et al., 2017) connects to the effect of granite on concrete because their bentonite–concrete cores were also influenced by the surrounding pore water during their preparation at the Grimsel Test Site (granitic formations of the Aar Massif, Switzerland). All of the other reviewed local and international works, which are more relevant for the study of granite–concrete interactions at the National Radioactive Waste Repository of Hungary, Bátaapáti, are modeling studies (Benő and Molnár, 2010; Chaparro et al., 2017; Fintor and Nagy, 2015; Nagy, 2015; Pfingsten et al., 2006; Soler and Mäder, 2007, 2010). Coupled experimental results are also available in some publications (Chaparro et al., 2017; Pfingsten et al., 2006; Soler and Mäder, 2007, 2010) in connection to the Grimsel Test Site. In these experiments, granitic cores are flooded by high-pH solutions representing the early stages in the degradation of cement (Pfingsten et al., 2006; Soler and Mäder, 2007, 2010) or hardened cement in a borehole is interacted with the Grimsel granitic groundwater (Chaparro et al., 2017).

Alonso et al. (2017) observed and described portlandite dissolution and the decalcification of CSH for the combined effect of bentonite and granitic pore waters in the concrete part of their bentonite–concrete interface sample. The study of Chaparro et al. (2017) focusing on the effects of Grimsel granitic pore water on hardened cement in a borehole, also showed portlandite dissolution in the postmortem analysis of samples and their coupled 1D model. This indicated an increase in porosity. However, their 2D model showed a reduction in porosity in the fault gouge due to secondary mineral precipitation. They described ettringite, CASH, hydrotalcite, calcite and illite formation at various locations in their model domain and calcite was responsible for porosity decrease with up to 40% of its value. In the other international studies the focus falls on the granite (Pfingsten et al., 2006; Soler and Mäder, 2007, 2010) where secondary precipitation of CSH, CASH and also zeolites, plus the decrease of hydraulic permeability (not necessarily connected to porosity but to pore geometry) were found for the effect of simulated high-pH cement pore water.

From the study area of present paper, the National Radioactive Waste Repository of Hungary, Bátaapáti, only 1D thermodynamic reactive transport modeling works are available, which focus on geochemical interactions between granite and concrete (Benő and Molnár, 2010; Fintor and Nagy, 2015; Nagy, 2015). They all report of the complete dissolution of modeled concretes in a time period between 5000 and 20000 years and the secondary precipitation of calcite around the contact to granite. It was mentioned that the calcite precipitation would also mean a significant drop in porosity and permeability, which could not be taken into account in these models. These works refer to the dissolution of portlandite as the Ca^{2+} source and the granitic pore water as the CO_2 source for calcite formation and also to the importance of the potential permeability changes on the outcome of model predictions. So far, no

Table 5
Qualitative ATR-FTIR results, i.e. detected phases in powder samples of granite (G), concrete (C), granite–concrete (GC) and concrete–concrete (CC) interface.

Powder sample/wt% of minerals		quartz	K-feldspar/plagioclase	mica/chlorite	Portlandite	gypsum	calcite/dolomite/vaterite
Granite	Bz-1521-G	X	X				X
	Bz-1621-G	X	X				
	Bz-1721-G	X	X				
	Bz-1753-G	X	X	X			
	Bz-1843-G	X	X	X			
Concrete	Bz-1521-C	X	X		X		X
	Bz-1531-C	X	X	X	X		X
	Bz-1533-C	X	X	X	X		X
	Bz-1542-C	X	X	X	X		X
	Bz-1621-C	X	X		X		X
		X	X		X		X
	Bz-1642-C	X	X	X	X		X
	Bz-1721-C	X	X		X		X
		X	X		X		X
	Bz-1753-C	X	X		X		X
	Bz-1812-C	X	X				X
	Bz-1843-C	X	X		X		X
	Bz-1862-C	X	X	X	X		X
Interface	Bz-1521-GC	X	X				X
	Bz-1621-GC	X	X			X	X
	Bz-1721-GC	X	X		X		X
	Bz-1843-GC	X	X	X	X		X

Table 6
Semi-quantitative TA results in comparison with corresponding XRD data (Table 4.), i.e. wt% proportions of TA detected phases in selected powder samples of concrete (C) and granite–concrete (GC) interface. Relative amounts of quartz are marked by + signs based on visual observations of the technician.

Powder sample/wt% of minerals		Quartz		chlorite		ettringite		portlandite		gypsum		calcite		dolomite	
		TA	*XRD*	TA	*XRD*	TA	*XRD*	TA	*XRD*	TA	*XRD*	TA	*XRD*	TA	*XRD*
Concrete	Bz-1521-C	+++	*55*			8	*8*	3	*4*			5	*5*	3	*2*
	Bz-1621-C	+++	*56*			10	*10*	4	*4*				*6*		
		+++	*59*			10	*10*	3	*4*			8	*4*		
	Bz-1721-C	+++	*53*	4	*4*	8	*8*	3	*4*				*8*		
		++	*50*			6	*4*	5	*5*			*7*	*8*		
	Bz-1753-C	+++	*46*			11	*10*	5	*6*			5	*5*	4	*3*
	Bz-1843-C	++	*51*			6	*4*	3	*4*			6	*5*	2	*3*
Interface	Bz-1521-GC	+	*35*			7	*5*	2	*2*			21	*21*		
	Bz-1621-GC	+	*41*			9	*8*			7	*6*		*13*		
	Bz-1721-GC	++	*37*	10	*9*	4	*4*	2	*3*				*5*		*2*
	Bz-1843-GC	+	*30*			2	*1*	2	*2*			31	*32*		

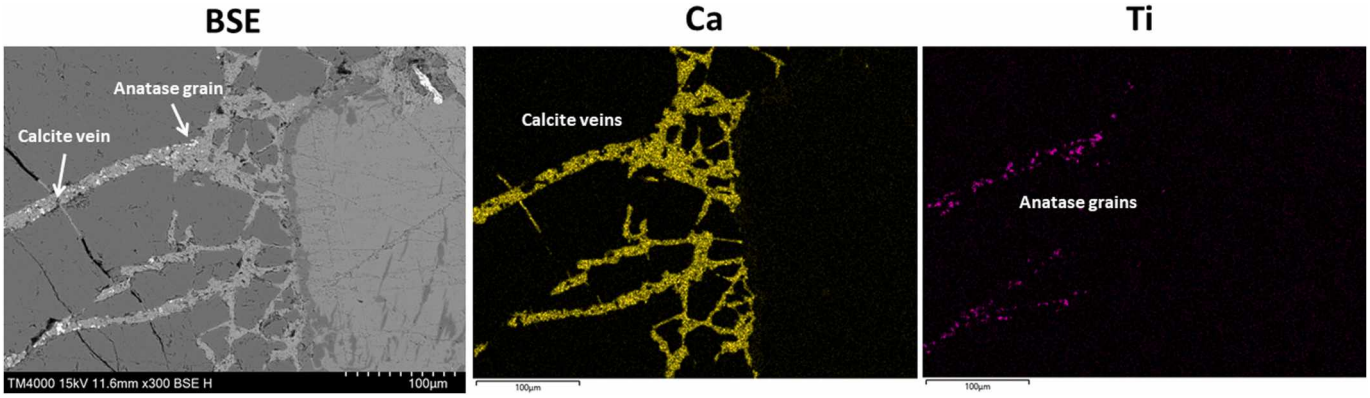

Fig. 4. Back scattered electron (BSE) image, Ca and Ti element maps of calcite veins in the granite with anatase grains. These images were made in the granite part of the thin section of Bz-1521 core.

experiments confirmed these modeling results.

5.2. Geochemical interactions between granite and concrete at Bátaapáti

5.2.1. Formation of Ca-carbonates near the interface

As detailed among the results, phase analyses showed the main phases to precipitate at the granite–concrete interface are calcite and vaterite (Section 4.1, Tables 4 and 6). Dolomite and aragonite are other carbonates detected (Tables 4 and 6). Imaging techniques confirmed the presence of significant volume of Ca-carbonates formed due to geochemical interactions of the rock and building material (Sections 4.2.1 and 4.2.4). Several examples were seen for calcite veins appearing along the contact with various thicknesses (Sections 4.2.1, Fig. 5). Ca-zonation is also observed in the fine grained concrete matrix by EDS

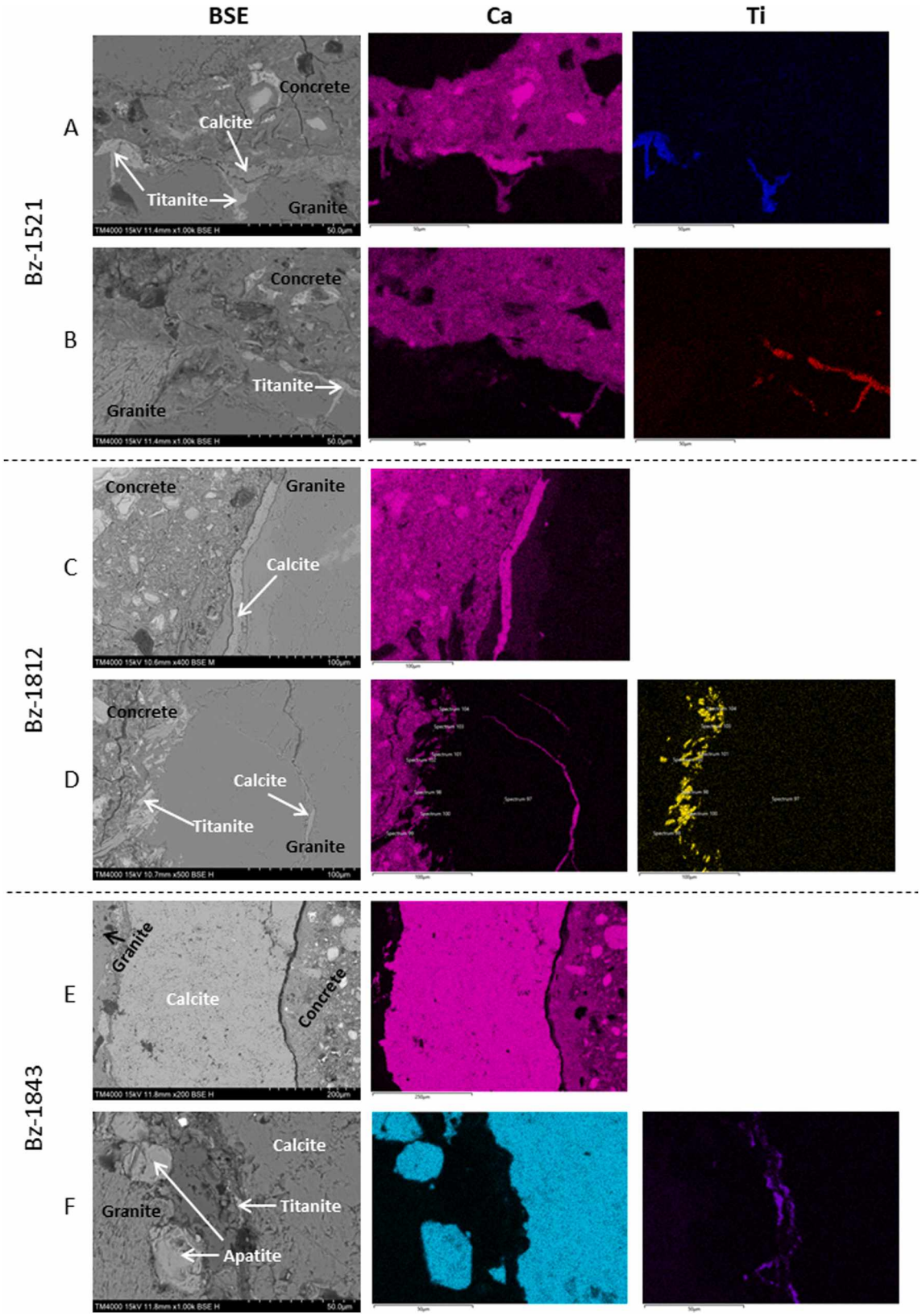

Fig. 5. BSE images, Ca and Ti element maps of calcite veins and titanite occurrences along or near the granite–concrete interface: A) granite at the bottom, concrete with aggregates at the top and calcite vein and titanite at the center from the thin section of Bz-1521 core, B) granite at the bottom, concrete at the top and titanite at the right center from the thin section of Bz-1521 core, C) concrete at the left, granite at the right and calcite vein at the center from the thin section of Bz-1812 core, D) concrete at the left, granite at the right, calcite vein in the granite connected to the interface and titanite right along the interface from the thin section of Bz-1812 core, E) granite at the left, concrete with two types of matrixes (lighter vs. darker on both types of images) at the right and a 400 μm thick calcite vein at the center from one of the thin sections of Bz-1843 core, F) granite with apatite grains at the left, the 400 μm thick calcite vein at the right (same as in Fig. 5E images) and titanite at the center from the Bz-1843 thin section. Other phases are not in the focus of present study.

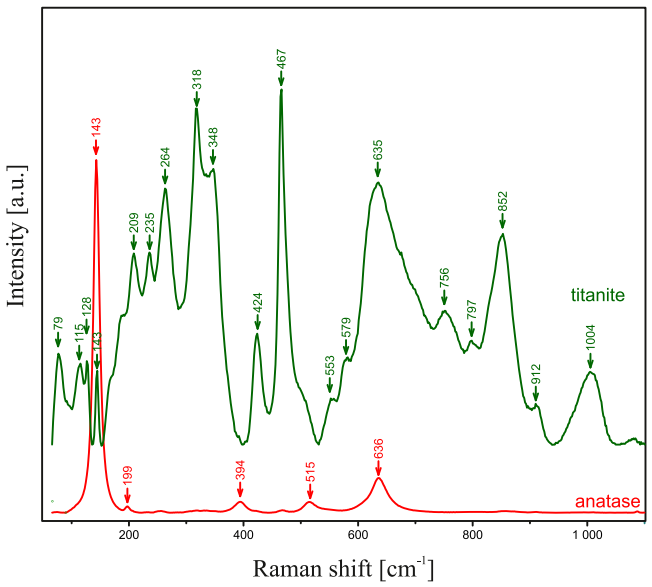

Fig. 6. Raman-spectra of detected Ti-bearing phases, anatase and titanite.

analysis with higher values close to the interface with granite and lower values further away (Section 4.2.4, Fig. 8). Raman-mapping (Fig. 8B) showed that the additional Ca in the enriched zone is present in the form of vaterite, which is precipitated in the pores of the concrete.

For the observed precipitation of Ca-carbonates at the interface of granite and concrete, Ca^{2+} must be present in the solution, which is most probably supplied by the dissolution of cement phases, mainly portlandite, as suggested in the literature (Section 5.1.1, Jenni et al., 2017; Lalan et al., 2019, 2016 and Section 5.1.2, Alonso et al., 2017; Benő and Molnár, 2010; Chaparro et al., 2017; Fintor and Nagy, 2015; Nagy, 2015). Plagioclase ($Na_{0.5}Ca_{0.5}Si_3AlO_8$) in granite, or the 30–40 mg/l Ca^{2+}-content of granitic pore water may also contribute to the availability of Ca^{2+} for carbonate formation near the interface. This could directly explain the observed Ca-zonation. However, if the Ca^{2+} comes from the cement/portlandite (which is more probable considering its significant Ca-content), the changes in the Ca-signal can be only explained by Ca-relocation from courser crystals (which were excluded from the analysis) to finer grains of vaterite (included in the cement matrix). Another requirement is the presence of dissolved CO_2 in the system. Since it does not have significant solid sources in the system, this can be satisfied by the local granitic pore waters at Bátaapáti, which contain about 350 mg/l HCO_3^- (Section 2, Benő and Molnár, 2010; Szabó et al., 2017). This assumption is also supported by the modeling works available from the study area (Benő and Molnár, 2010; Fintor and Nagy, 2015; Nagy, 2015), which all predict significant secondary calcite precipitation at the entry of dissolved CO_2 in the granitic pore water.

Besides calcite formation indicated in all modeling works for the study area (Benő and Molnár, 2010; Fintor and Nagy, 2015; Nagy, 2015), a number of the other reviewed articles (Bernard et al., 2020; Fernández et al., 2017; Jenni et al, 2014, 2017; Lalan et al, 2016, 2019) also report heterogeneous, zoned or diffuse carbonation (carbonate, mostly calcite precipitation) at the interface of clayey and cementitious materials. Among the studies focusing on especially granitic rocks, Chaparro et al. (2017) also described calcite and other secondary mineral formation in their 2D model, among which calcite precipitated in the highest volume. These all support the idea that Ca-carbonates at the granite–concrete interface in the samples of this study formed due to geochemical interactions between the rock and building material and that the calcite veins seen at the contact are not related to the original hydrothermal calcite veins in Mórágy Granite Formation. This means

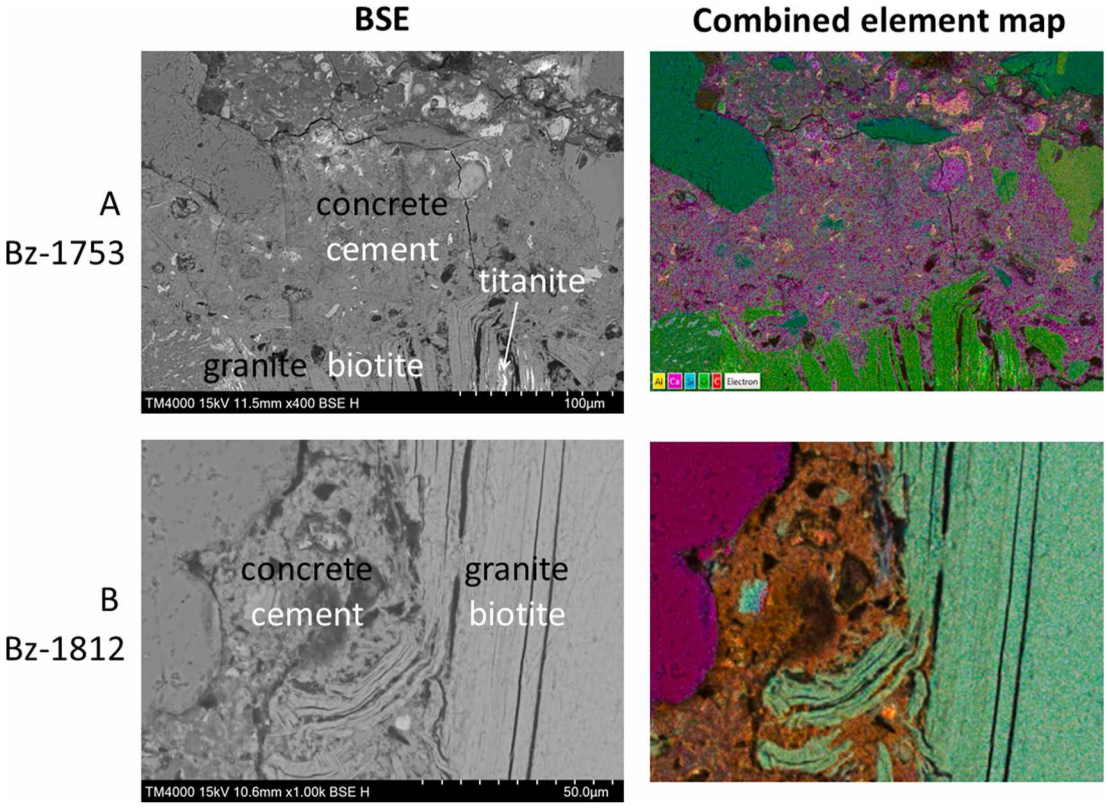

Fig. 7. BSE images, and combined element maps about concrete matrix, cement intrusion into biotite minerals of granite: A) concrete at the top, and biotite with bright anatase grains at the bottom, and concrete within its cleavage directions from the thin section of Bz-1753 core, B) concrete with aggregates at the left and biotite with concrete within its layers at the right from the thin section of Bz-1812 core.

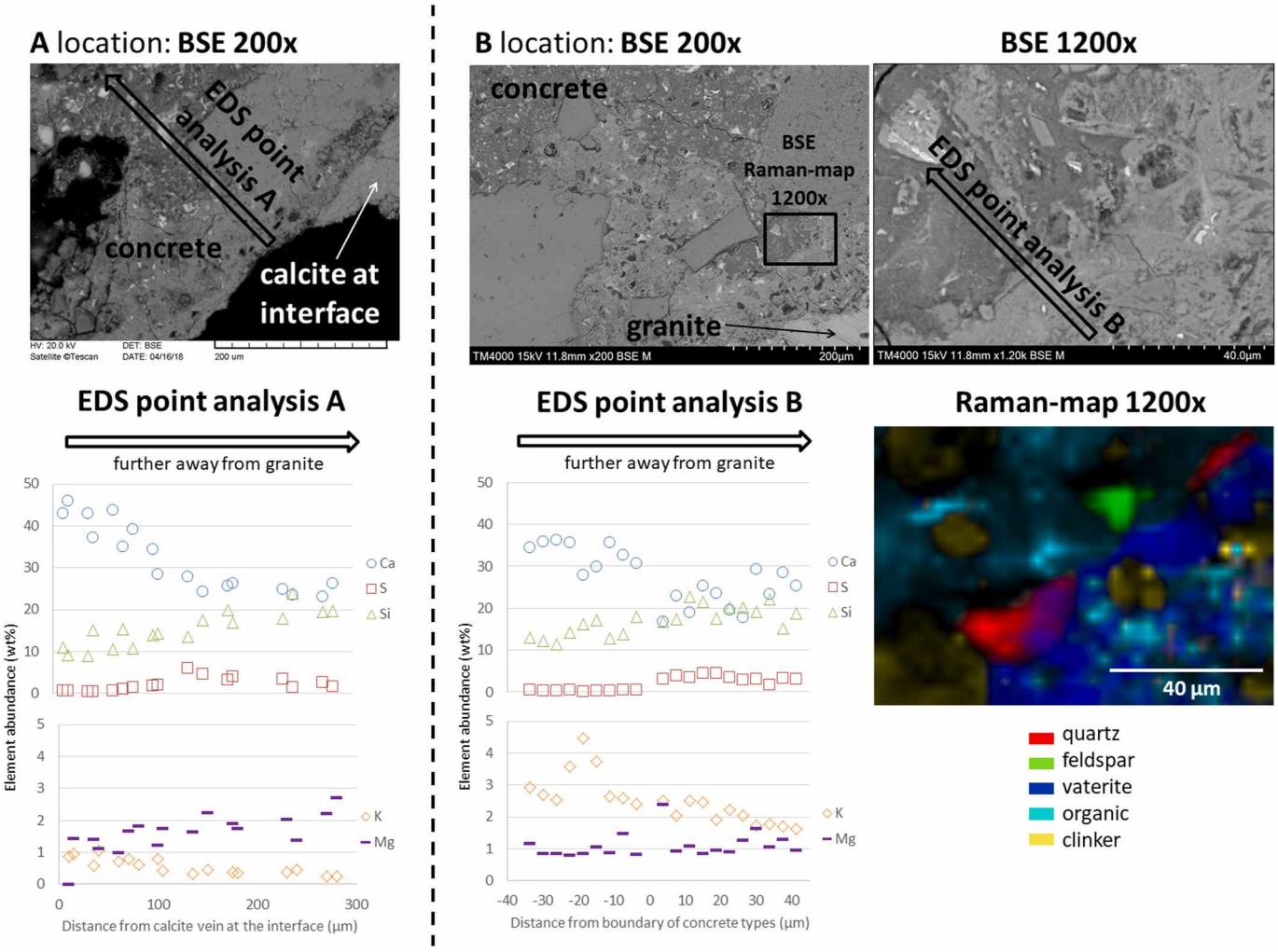

Fig. 8. *BSE images, EDS results and Raman-map of the two types of concrete matrix occurring frequently along the granite contact (dark vs. light grey in BSE images): A) results from the thin section of Bz-1843 core (modified after Szabó-Krausz et al., 2019) and B) results from the thin section of Bz-1531 core. The EDS data focus only on the elements with visible variability.*

that the new voids, fractures formed during the construction of the repository are filled up with solid materials and clogged, which is advantageous for minimizing the migration of fluids in the system.

Vaterite precipitation in the pores of concrete, near the contact with granite (Section 4.2.4, Fig. 8) is one of the most important results achieved in this study, even though it is not unique since vaterite was also found in e.g. concrete/argillite interfaces of De Windt et al. (2008). Vaterite is thermodynamically the least stable anhydrous polymorph of $CaCO_3$ at ambient conditions (Radha and Navrotsky, 2013). Even though, it is expected to transform into calcite with time (Radha and Navrotsky, 2013), the question rises why calcite veins are formed but vaterite fills the pores of concrete. At the temperature conditions of the repository (17–18 °C plus concrete hydration heat), $CaCO_3$ precipitation is possible as both calcite and vaterite at the early metastable stage (Trushina et al., 2014). What probably causes that vaterite precipitation is favored over calcite in concrete pores is the certainly very high activity product of calcium at these locations (Kawano et al., 2009).

The formation of vaterite is important, because similarly to calcite veins, which reduce the fluid flow along fractures, vaterite acts as a pore filling mineral, which also reduces the porosity and permeability. In several studies, the observed carbonation is linked to a decrease in porosity, i.e. pore clogging (Bernard et al., 2020; Jenni et al, 2014, 2017; Lalan et al, 2016, 2019). It is described that this process may avoid further alteration of the materials in greater depths. The 2D model of Chaparro et al. (2017) also showed a reduction in porosity in the fault gouge by 40% of its value. The modeling works from the study area (Benő and Molnár, 2010; Fintor and Nagy, 2015; Nagy, 2015) could not yet take into account porosity changes, however they mention that they would expect a significant drop in porosity and permeability due to calcite formation near the granite-concrete interface. These authors did not separate calcite and vaterite since vaterite is metastable in these conditions and it will revert to calcite over time (Ishikawa et al., 2003; Radha and Navrotsky, 2013; Skinner and Ehrlich, 2014). Present study, therefore, supports their assumptions with experimental data.

5.2.2. *Transformation of Ti-phases in the studied system*

Any of the reviewed interface (Section 5.1.1) or granite–concrete interaction studies (Section 5.1.2) did not report about observations regarding Ti-minerals, such as anatase and titanite in this study (Section 4.2.2, Fig. ***6***). Titanite was frequently observed along or near the granite–concrete interface, in the granite side (Fig. 5A, B, D and F). Not all Ti-occurrences near the interface are identified as titanite (Section 4.2.2), but sometimes anatase. Still, titanite looks to be a quite typical phase to form. When calcite vein appears between granite and concrete due to their interaction (Section 5.2.1), titanite may also be present; in these cases, it is between the calcite vein and the granite (Fig. 5A and F). This suggests that as the granitic pore water reacts with concrete, first a minor amount of titanite forms and then calcite (and vaterite) as the

reactions front moves ahead to concrete.

To better understand possible reactions of Ti-phases, an important recent study to consider is that of Novoselov et al. (2020). It reveals the thermodynamically-driven conversion from calcite to titanite at elevated ambient temperatures (Campinas region, São Paulo state, Brazil, 16–27 °C, Novoselov et al., 2020). Similar temperatures, 17–18 °C characterize as well the National Radioactive Waste Repository of Hungary at around 275 m depth from the surface. Novoselov et al. (2020) found this despite that "a number of authors argued that titanite is unstable at ambient conditions and cannot be formed at temperatures <100 °C or <60 °C". They also describe that the chemical stability of titanite depends on the pressure, temperature and the presence of H^+, HCO_3^-, Ca^{2+}, dissolved SiO_2 and that higher temperatures and pH or lower CO_2 partial pressures are favorable for the formation of this phase. Following Hunt and Kerrick (1977), the reaction can be written as $TiO_2 + CaCO_3 + SiO_2 = CaTiSiO_5 + CO_2$, where CO_2 refers to the total dissolved carbon-dioxide including HCO_3^- and CO_3^{2-}. This reaction equation also supports that "the deposition of carbonate minerals is thermodynamically avoided at the stability field of titanite" (Novoselov et al., 2020).

Consequently, titanite may form in the studied granite–concrete system, where carbonates cannot but still there is enough Ca^{2+} and dissolved SiO_2 in the fluid, as well as, a source of TiO_2. Calcium and SiO_2 may come from the concrete and TiO_2 comes from the granite. This latter is supported by the results of 0.1–0.2 wt% TiO_2 detected in concrete most probably present in granite fragments as aggregates (Table 3) and of Ti-phases observed in the granite, like anatase (Fig. 4) and titanite (Fig. 7A). Descriptive works from the area also report of titanium-bearing phases in the granite, which are mainly identified as titanite and connect to biotite mineral (Balla et al., 2009; Király, 2010; Király and Koroknai, 2004). In the studied cementitious system a pH > 12 and an Eh (redox potential) > −0.8 V situation can be imagined, where the otherwise quite stable titanium forms $HTiO_3^-$ ions in solution and mobilizes (Alexander, 2016; Bhola and Mishra, 2013).

Calcite veins filling voids between granite and concrete, and vaterite precipitated in the pores of concrete near the contact with granite, both require the presence of HCO_3^- in the solution. Titanite is possible to be stable when and where the HCO_3^- concentration drops, probably used up for carbonate formation. Therefore, we may see carbonate and titanite formation next to each other (Fig. 5A and F) because geochemical and thermodynamical constrains change within short distances at the granite–concrete interface as reaction front. This is also supported by the idea of Ti-release from granite and precipitation within a very short distance near the interface. As a summary, it seems that both pH and dissolved CO_2 content of pore water have a role in titanite precipitation at the interface. First the high pH (≈12–14) affects granite and more titanium mobilizes. Then calcite and vaterite forms, which reduce the dissolved CO_2 content in the pore water and locally titanite can precipitate. Better understanding of these reactions can be achieved by improved reactive transport modeling of the system and in return, taking into account Ti-phases in these models of the repository may also support their validity.

5.2.3. Possible factors in the granite–concrete attachment

Two main types of core samples can be separated depending on the attachment of granite and concrete, i.e. if they are grown together or not (Fig. 2, Table 1). The question rises, what circumstances may potentially cause this difference. Looking at the sampling location, which can potentially be connected to the fluid flows, no relationship was observed (Table 1, Fig. 1B) alike for the ages of interfaces (Table 1). The significant formation of Ca-carbonates near the contact (Section 5.2.1) does not seem to show variability according to the attachment type either (Table 4). Therefore, this process is probably not the responsible one for granite and concrete merging.

Analyses of thin sections by SEM-EDS pointed out that when granite and concrete are attached, along cleavage plains, cementitious material penetrates the sheets of biotite, which is one of the most common granite minerals. These results were detailed in Section 4.2.3 and seen in Fig. 7. Mica/biotite is detected by XRD in average 11 ± 7 wt% (Section 4.1., Table 4). Therefore, biotite enough frequently must appear right at the granite–concrete contact to be able to make a significant impact. The probability of cement penetration into biotite must connect to the abundance of this mineral in the granite at the given location. Since the granite is heterogeneous in decimeter scale, the presence of biotite might govern the attachment of granite and concrete in the cores. Looking at the biotite content of granite part of cores (Table 4), the non-attached samples have a biotite content of 6 ± 2 wt% in average, whereas the cores which are grown together show 14 ± 7 wt%. However, one sample out of 11 (Bz-1721-G, Table 4) shows exceptionally low biotite content (3 wt%) even though the granite and concrete are grown together. If this sample is taken out from the statistics the latter average rises up to 16 ± 6 wt%. Therefore, the attached core samples show more than the double biotite abundance than the non-attached ones. This observation supports the idea that the local abundance of biotite in the heterogeneous granite will decide if the core sample is grown together or not because the cementitious material has a capability to penetrate among the layers of the phyllosilicate biotite even up to several tens μm away from the contact (Section 4.2.3., Fig. 7).

5.2.4. Possibility of other elemental zonation in concrete matrix

The SEM-EDS analysis (Section 4.2.4.) showed that with the distance from the granite contact, the Ca- and K-contents of the cement matrix are decreasing, whereas its Si-, S- and Mg-contents are increasing (Fig. 8). Zonation of Si, S and Mg may refer to important signs of granite–concrete interactions.

Close to the interface, the Si-abundance in concrete seems to decrease (Fig. 8). C(A)SH is the most important Si-bearing phase in hydrated cement. It was not detected in this study because of its presumably low crystallinity, however, the observed variation in Si-content might connect to the reactions of C(A)SH. A drop in Si-content either refers to the transformation of C(A)SH to its higher Ca/Si ratio forms or to its dissolution. However, it is contradicting that most studies (Section 5.1) either describe the decalcification (Alonso et al., 2017) or the formation of this amorphous phase (Chaparro et al., 2017; Fernández et al., 2006; Lalan et al, 2016, 2019; Lerouge et al., 2017; Pfingsten et al., 2006; Soler and Mäder, 2007, 2010). Although, a few studies (Alonso et al., 2017; Bernard et al., 2020) support the hypothesis of C(A)SH dissolution by reporting about its alteration. Models from the study area (Benő and Molnár, 2010; Fintor and Nagy, 2015; Nagy, 2015) also predict this scenario, but it still remains questionable that the C(A)SH dissolution is seen in the recorded data (Fig. 8). A technical explanation can be also given to the observed Si-zonation; due to vaterite precipitation in the pores (Sections 4.2.4 and 5.2.1, Fig. 8) the Si-signal gets diluted.

Closer to the interface with granite, the S-abundance also seems to drop in cement matrix (Fig. 8). Again, technical reasons might be able to cause this observation that vaterite pore filling induced signal dilution. However, it is also possible that it indicates reactions, dissolution near the contact of the most important sulfate phase in cement, namely ettringite. The latter scenario is also supported by the observation of another sulfate mineral, gypsum, in one of the interface powder samples confirmed by all the analytical techniques used (Tables 4–6). Sulfate precipitation at the interface has also been observed by Lerouge et al. (2017). Jenni et al. (2017, 2014) and Bernard et al. (2020) also observed that SO_4^{2-} diffused away from or dissolved near the interface in their samples, similarly to the indicated reactions in this work.

Similarly to Si- and S- contents, Mg-distribution in cement matrix display lower values near the contact and higher further away. This observation is not similar to any of the results of reviewed articles which mainly report of Mg enrichment and the precipitation of Mg-phases near their interfaces (Section 5.1.1) (Bernard et al., 2020; Dauzeres et al., 2016; Fernández et al., 2017; Lerouge et al., 2017) or migration of Mg

into the cementitious phase (Alonso et al., 2017; Jenni et al, 2014, 2017).

6. Conclusions

In present work three main signs of geochemical interactions were observed at the granite–concrete interface samples from the National Radioactive Waste Repository of Hungary, Bátaapáti:

The main secondary phases at the interface are Ca-carbonates, i.e. calcite and vaterite. Phase analytical results, SEM-EDS analysis and Raman-spectroscopy confirmed that calcite veins appear along the granite–concrete contact and that vaterite precipitates in the pores of concrete near the interface. This carbonation happens with the available Ca^{2+} from the dissolution of cement and HCO_3^- from the local granitic pore water. This process reduces the porosity and permeability avoiding or slowing down further interaction of the materials at greater depths. These observations are in agreement with international literature and are also supported by previous modeling works from the study area. These modeling works are recommended to be improved with these considerations.

The second sign of interaction is the frequent detection of titanite, by SEM-EDS and Raman-spectroscopy, along or near the granite–concrete interface, always on the side of granite, sometimes between the formed calcite vein and the granite. It has been concluded that titanite forms in the studied system where concentration of Ca^{2+} is not high enough to form carbonates and it has dissolved SiO_2 in the solution, and the granite serves as a source of TiO_2. Therefore, the observations of neighboring calcite and titanite precipitations indicate that geochemical and thermodynamical constrains change within short distances at the reaction front (i.e., the granite–concrete interface). Based on the observations of present study, it is suggested to take Ti-bearing phases into account in further modeling works of the repository, as tracers of geochemical interactions.

The third sign connects to the two main types of granite–concrete cores: cores in which granite and concrete are grown together along the interface or cores in which they are not grown together, but their interface can be reconstructed. Based on phase analytical and SEM-EDS results, the inhomogeneous distribution of biotite mineral in granite will decide if the core sample is grown together or not. This is because the cementitious material has a capability to penetrate among the sheets of this phyllosilicate several tens of μm depth, which process causes the attachment if there is enough biotite around.

Declaration of competing interest

The authors declare that they have no known competing financial interests or personal relationships that could have appeared to influence the work reported in this paper.

Acknowledgements

This study is done within the framework of project Prémium_2017-13 lead by Zsuzsanna Szabó-Krausz, titled “Geochemical interactions of concrete in core samples, experiments and models”, financed by the Premium Postdoctorate Research Program of the Hungarian Academy of Sciences, later the Eötvös Loránd Research Network. This work was furthermore supported by the Mining and Geological Survey of Hungary and the ELTE Institutional Excellence Program (1783–3/2018/FEKUTSRAT) funded by the Hungarian Ministry of Human Capacities. The core samples were provided by the Public Limited Company for Radioactive Waste Management. Thanks goes to the members of the Mining and Geological Survey of Hungary, the Lithosphere Fluid Research Lab and the Research and Industrial Relations Center, Faculty of Science, Eötvös Loránd University. The authors especially thank the contribution of Ábel Szabó, Ágnes Freiler-Nagy, Anikó Besnyi, Árpádné Szabó, Beatrix Udvardi, Edit Király, Gáborné Menich, István Gatter, Judit Füri, Judit Turi, Nóra Edit Gál, Tamás Spránitz, Zoltán Dankházi, Zoltán Kovács, Zsolt Horváth. Additionally, the authors are very thankful for the insightful review of the two anonymous reviewers, which helped to improve the manuscript significantly.

References

Alexander, J.C., 2016. Appendix B, phase diagrams of TiO2 and H2O, surface modifications and growth of titanium dioxide for photo-electrochemical water splitting. https://doi.org/10.1007/978-3-319-34229-0.

Alonso, M.C., García Calvo, J.L., Cuevas, J., Turrero, M.J., Fernández, R., Torres, E., Ruiz, A.I., 2017. Interaction processes at the concrete-bentonite interface after 13 years of FEBEX-Plug operation. Part I: concrete alteration. Phys. Chem. Earth 99, 38–48. https://doi.org/10.1016/j.pce.2017.03.008.

Balla, Z., Császár, G., Gulácsi, Z., Gyalog, L., Kaiser, M., Király, E., Koloszár, L., Koronkai, B., Magyari, A., Maros, G., Marsi, I., Molnár, P., Rotárné Szalkai, Á., Tóth, G., 2009. A Mórágyi-Rög Északkeleti Részének Földtana - Magyarország Tájegységi Térképsorozata - Magyarázó a Mórágyi-Rög ÉK-I Részének Földtani Térképsorozatához (1:10 000). Geological Institute of Hungary, Budapest, Hungary.

Balmer, S., Kaufhold, S., Dohrmann, R., 2017. Cement-bentonite-iron interactions on small scale tests for testing performance of bentonites as a barrier in high-level radioactive waste repository concepts. Appl. Clay Sci. 135, 427–436. https://doi.org/10.1016/J.CLAY.2016.10.028.

Beno, E., Molnar, P., 2010. Valós Betonösszetétel Alapján Meghatározott Anyag Hidratációjának És Degradációjának Modellezése a Tároló Környezetében Található Rétegvizekre Jellemző Hidrogeokémiai Környezetben, RHK-K-192/09 Report.

Bernard, E., Jenni, A., Fisch, M., Grolimund, D., Mäder, U., 2020. Micro-X-ray diffraction and chemical mapping of aged interfaces between cement pastes and Opalinus Clay. Appl. Geochem. 115 https://doi.org/10.1016/J.APGEOCHEM.2020.104538, 104538.

Bhola, S.M., Mishra, B., 2013. Effect of ph on the electrochemical properties of oxides formed over β - Ti-15Mo and mixed Ti-6Al-4v alloys. Int. J. Electrochem. Sci. 8, 7075–7087.

Buil, B., Gómez, P., Peña, J., Garralón, A., Turrero, M.J., Escribano, A., Sánchez, L., Durán, J.M., 2010. Modelling of bentonite-granite solutes transfer from an in situ full-scale experiment to simulate a deep geological repository (Grimsel Test Site, Switzerland). Appl. Geochem. 25, 1797–1804. https://doi.org/10.1016/j.apgeochem.2010.09.003.

Chaparro, M.C., Saaltink, M.W., Soler, J.M., 2017. Reactive transport modelling of cement-groundwater-rock interaction at the Grimsel Test Site. Phys. Chem. Earth 99, 64–76. https://doi.org/10.1016/j.pce.2017.05.006.

Dauzeres, A., Achiedo, G., Nied, D., Bernard, E., Alahrache, S., Lothenbach, B., 2016. Magnesium perturbation in low-pH concretes placed in clayey environment - solid characterizations and modeling. Cement Concr. Res. 79, 137–150. https://doi.org/10.1016/j.cemconres.2015.09.002.

De Windt, L., Marsal, F., Tinseau, E., Pellegrini, D., 2008. Reactive transport modeling of geochemical interactions at a concrete/argillite interface, Tournemire site (France). Phys. Chem. Earth 33, 295–305. https://doi.org/10.1016/j.pce.2008.10.035.

Fernández, R., Cuevas, J., Sánchez, L., de la Villa, R.V., Leguey, S., 2006. Reactivity of the cement–bentonite interface with alkaline solutions using transport cells. Appl. Geochem. 21, 977–992. https://doi.org/10.1016/J.APGEOCHEM.2006.02.016.

Fernández, R., Torres, E., Ruiz, A.I., Cuevas, J., Alonso, M.C., García Calvo, J.L., Rodríguez, E., Turrero, M.J., 2017. Interaction processes at the concrete-bentonite interface after 13 years of FEBEX-Plug operation. Part II: bentonite contact. Phys. Chem. Earth 99, 49–63. https://doi.org/10.1016/j.pce.2017.01.009.

Fintor, K., Nagy, T., 2015. A Hazai Kis- És Közepes Aktivitású Nukleáris Hulladéklerakó Konténer Betonja Hosszú Távú Degradációjának Geokémiai Modellezése. In: Pál-Molnár, E., Raucsik, B., Varga, A. (Eds.), Meddig Ér a Takarónk? A Magmaképződéstől a Regionális Litoszféra Formáló Folyamatokig: 6. Kőzettani És Geokémiai Vándorgyűlés. University of Szeged, Szeged, Hungary, p. 46.

Gautam, P.K., Verma, A.K., Singh, T.N., Hu, W., Singh, K.H., 2019. Experimental investigations on the thermal properties of Jalore granitic rocks for nuclear waste repository. Thermochim. Acta 681. https://doi.org/10.1016/J.TCA.2019.178381, 178381.

Hedin, A., Olsson, O., 2016. Crystalline rock as a repository for Swedish spent nuclear fuel. Elements 12, 247–252. https://doi.org/10.2113/gselements.12.4.247.

Hunt, J.A., Kerrick, D.M., 1977. The stability of sphene; experimental redetermination and geologic implications. Geochem. Cosmochim. Acta 41, 279–288. https://doi.org/10.1016/0016-7037(77)90236-8.

Idiart, A., Laviña, M., Kosakowski, G., Cochepin, B., Meeussen, J.C.L., Samper, J., Mon, A., Montoya, V., Munier, I., Poonoosamy, J., Montenegro, L., Deissmann, G., Rohmen, S., Damiani, L.H., Coene, E., Nieves, A., 2020. Reactive transport modelling of a low-pH concrete/clay interface. Appl. Geochem. 115 https://doi.org/10.1016/j.apgeochem.2020.104562.

Ishikawa, K., Matsuya, S., Miyamoto, Y., Kawate, K., 2003. In: Milne, I., Ritchie, R.O., Karihaloo, B.B.T.-C.S.I. (Eds.), 9.05 - Bioceramics. Pergamon, Oxford, pp. 169–214. https://doi.org/10.1016/B0-08-043749-4/09146-1.

Jenni, A., Mäder, U., Lerouge, C., Gaboreau, S., Schwyn, B., 2014. In situ interaction between different concretes and Opalinus Clay. Phys. Chem. Earth 70 (71), 71–83. https://doi.org/10.1016/j.pce.2013.11.004.

Jenni, A., Gimmi, T., Alt-Epping, P., Mäder, U., Cloet, V., 2017. Interaction of ordinary Portland cement and Opalinus Clay: dual porosity modelling compared to experimental data. Phys. Chem. Earth 99, 22–37. https://doi.org/10.1016/j.pce.2017.01.004.

Jo, Y., Chang, C., Ji, S.-H., Park, K.-W., 2019. In situ stress states at KURT, an underground research laboratory in South Korea for the study of high-level radioactive waste disposal. Eng. Geol. 259 https://doi.org/10.1016/J.ENGGEO.2019.105198, 105198.

Kawano, J., Shimobayashi, N., Miyake, A., Kitamura, M., 2009. Precipitation diagram of calcium carbonate polymorphs: its construction and significance. J. Phys. Condens. Matter 21, 425102. https://doi.org/10.1088/0953-8984/21/42/425102.

Kereki, F., 2016. Radioaktív hulladékok magyarországi kezelése és elhelyezése. Magy. Tudomany. http://www.matud.iif.hu/2016/05/02.htm.

Király, E., 2010. Magmatic Evolution of the Mórágy Granite (SE Transdanubia, Hungary) - Annual Report of the. Geological Institute of Hungary, 2009.

Király, E., Koroknai, B., 2004. The Magmatic and Metamorphic Evolution of the North-Eastern Part of the Mórágy Block - Annual Report of the Geological Institue of Hungary 2003.

Koťátková, J., Zatloukal, J., Reiterman, P., Kolář, K., 2017. Concrete and cement composites used for radioactive waste deposition. J. Environ. Radioact. 178– 179, 147–155. https://doi.org/10.1016/j.jenvrad.2017.08.012.

Lalan, P., Dauzères, A., De Windt, L., Bartier, D., Sammaljärvi, J., Barnichon, J.D., Techer, I., Detilleux, V., 2016. Impact of a 70 °c temperature on an ordinary Portland cement paste/claystone interface: an in situ experiment. Cement Concr. Res. 83, 164–178. https://doi.org/10.1016/j.cemconres.2016.02.001.

Lalan, P., Dauzères, A., De Windt, L., Sammaljärvi, J., Bartier, D., Techer, I., Detilleux, V., Siitari-Kauppi, M., 2019. Mineralogical and microstructural evolution of Portland cement paste/argillite interfaces at 70 °C – considerations for diffusion and porosity properties. Cement Concr. Res. 115, 414–425. https://doi.org/10.1016/j.cemconres.2018.09.018.

Lerouge, C., Gaboreau, S., Grangeon, S., Claret, F., Warmont, F., Jenni, A., Cloet, V., Mäder, U., 2017. In situ interactions between opalinus clay and low alkali concrete. Phys. Chem. Earth 99, 3–21. https://doi.org/10.1016/j.pce.2017.01.005.

Lu, C., Samper, J., Luis Cormenzana, J., Ma, H., Montenegro, L., Ángel Cuñado, M., 2012. Reactive transport model and apparent K d of Ni in the near field of a HLW repository in granite. Comput. Geosci. 49, 256–266. https://doi.org/10.1016/j.cageo.2012.06.003.

Mariner, P.E., Lee, J.H., Hardin, E.L., Hansen, F.D., Freeze, G.A., Lord, A.S., Goldstein, B., Price, R.H., 2011. Granite Disposal of U.S. High-Level Radioactive Waste. SANDIA REPORT. SAND2011-6203.

Maros, G., Borsody, J., Füri, J., Koroknai, B., Palotás, K., Rálischné Felgenhauer, E., 2012. A Mórágyi-Rög ÉK-I Részének Szerkezetföldtani Értékelése a Töréses Szerkezetekre.

Moghissi, A.A., 2006. The origin of the EPA's 10,000-year time frame for the high-level waste repository. Nucl. News 49, 41–42.

Murray, R.L., Holbert, K.E., Murray, R.L., Holbert, K.E., 2020. Radioactive waste disposal. Nucl. Energy 439–470. https://doi.org/10.1016/B978-0-12-812881-7.00023-X.

Nagy, T., 2015. A Bátaapáti Radioaktív Hulladéktároló Konténer Betonjának Hosszú Távú Degradációjának Geokémiai Modellezése. M.Sc thesis. University of Szeged.

Nehme, S.G., 2013. Construction Plan - A Bátaapáti Nemzeti Radioaktívhulladék-Tároló Térkiképzése - KIVITELI TERV, III. Ütem, 2. Szakasz - I-K3 És I-K4 Kamrák Kihajtására - Lövelltbeton Technológiai Terv AJKUN00001D003. Budapest, Hungary.

Novoselov, A.A., Silva, D., de Souza Filho, C.R., 2020. Authigenic titanite in weathered basalts: implications for paleoatmospheric reconstructions. Geosci. Front. 11 (6), 2183–2196. https://doi.org/10.1016/J.GSF.2020.03.012.

Parneix, J.C., 1992. Effects of hydrothermal alteration on radioelement migration from a hypothetical disposal site for high level radioactive waste: example from the Auriat granite. France. Appl. Geochemistry 7, 253–268. https://doi.org/10.1016/S0883-2927(09)80080-2.

Pfingsten, W., Paris, B., Soler, J.M., Mäder, U.K., 2006. Tracer and reactive transport modelling of the interaction between high-pH fluid and fractured rock: field and laboratory experiments. J. Geochem. Explor. 90, 95–113. https://doi.org/10.1016/J.GEXPLO.2005.09.009.

Radha, A.V., Navrotsky, A., 2013. Thermodynamics of carbonates. Rev. Mineral. Geochem. 77, 73–121. https://doi.org/10.2138/rmg.2013.77.3.

Samper, J., Naves, A., Montenegro, L., Mon, A., 2016. Reactive transport modelling of the long-term interactions of corrosion products and compacted bentonite in a HLW repository in granite: uncertainties and relevance for performance assessment. Appl. Geochem. 67, 42–51. https://doi.org/10.1016/j.apgeochem.2016.02.001.

Sika, 2019. PRODUCT DATA SHEET - Sika ® Sigunit ® L-54 AF.

Siren, T., Hakala, M., Valli, J., Kantia, P., Hudson, J.A., Johansson, E., 2015. In situ strength and failure mechanisms of migmatitic gneiss and pegmatitic granite at the nuclear waste disposal site in Olkiluoto, Western Finland. Int. J. Rock Mech. Min. Sci. 79, 135–148. https://doi.org/10.1016/J.IJRMMS.2015.08.012.

on G. Skinner, H.C.W., Ehrlich, H., 2014. 10.4 - biomineralization. In: Holland, H.D., Turekian, K.K.B.T.-T., Second, E. (Eds.). Elsevier, Oxford, pp. 105–162. https://doi.org/10.1016/B978-0-08-095975-7.00804-4.

Soler, J.M., 2012. High-pH plume from low-alkali-cement fracture grouting: reactive transport modeling and comparison with pH monitoring at ONKALO (Finland). Appl. Geochem. 27, 2096–2106. https://doi.org/10.1016/J.APGEOCHEM.2012.05.014.

Soler, J.M., Mäder, U.K., 2007. Mineralogical alteration and associated permeability changes induced by a high-pH plume: modeling of a granite core infiltration experiment. Appl. Geochem. 22, 17–29. https://doi.org/10.1016/J.APGEOCHEM.2006.07.015.

Soler, J.M., Mäder, U.K., 2010. Cement-rock interaction: infiltration of a high-pH solution into a fractured granite core. Geol. Acta 8, 221–233. https://doi.org/10.1344/105.000001531.

Soler, J.M., Vuorio, M., Hautojärvi, A., 2011. Reactive transport modeling of the interaction between water and a cementitious grout in a fractured rock. Application to ONKALO (Finland). Appl. Geochem. 26, 1115–1129. https://doi.org/10.1016/J.APGEOCHEM.2011.04.001.

Szabó, Z., Falus, G., Udvardi, B., Kónya, P., Gál, N.E., Király, E., Horváth, Z., Beke, Z., Besnyi, A., 2017. 7.5. A Kőzet-Víz-Építőanyag Rendszer Geokémiai Kölcsönhatásai - Midyear Report of the Geological Institue of Hungary 2017.

Szabó-Krausz, Z., Falus, G., Király, C., Török, P., Kovács, Z., Szabó, C., 2019. In-situ Interactions at the Granite-Concrete Interface of the National Radioactive Waste Repository, Hungary: Core Samples and Numerical models., in: Proceedings of the 15th International Congress on the Chemistry of Cement. Prague, Czech Republic, p. 6.

Szabó-Krausz, Z., Gál, N.E., Gável, V., Falus, G., 2020. Wellbore cement alteration during decades of abandonment and following CO2 attack – a geochemical modelling study in the area of potential CO2 reservoirs in the Pannonian Basin. Appl. Geochem. 113, 104516 https://doi.org/10.1016/j.apgeochem.2019.104516.

Tóth, M., T, 2018. Fracture network characterization using 1D and 2D data of the Mórágy Granite body, southern Hungary. J. Struct. Geol. 113, 176–187. https://doi.org/10.1016/j.jsg.2018.05.029.

Trushina, D.B., Bukreeva, T.V., Kovalchuk, M.V., Antipina, M.N., 2014. CaCO3 vaterite microparticles for biomedical and personal care applications. Mater. Sci. Eng. C 45, 644–658. https://doi.org/10.1016/j.msec.2014.04.050.

Wang, J., Chen, L., Su, R., Zhao, X., 2018. The Beishan underground research laboratory for geological disposal of high-level radioactive waste in China: planning, site selection, site characterization and in situ tests. J. Rock Mech. Geotech. Eng. 10, 411–435. https://doi.org/10.1016/J.JRMGE.2018.03.002.

Yoshida, H., Aoki, K., Semba, T., Ota, K., Amano, K., Hama, K., Kawamura, M., Tsubota, K., 2000. Overview of the stability and barrier functions of the granitic geosphere at the Kamaishi Mine: relevance to radioactive waste disposal in Japan. Eng. Geol. 56, 151–162. https://doi.org/10.1016/S0013-7952(99)00140-4.

Zuo, J.-P., Wang, J.-T., Sun, Y.-J., Chen, Y., Jiang, G.-H., Li, Y.-H., 2017. Effects of thermal treatment on fracture characteristics of granite from Beishan, a possible high-level radioactive waste disposal site in China. Eng. Fract. Mech. 182, 425–437. https://doi.org/10.1016/J.ENGFRACMECH.2017.04.043.